INFORMATICS JOURNALS
The Journal of Electrochemical Society of India, *Volume 74, Issue (1&2), January – March 2025; pp. 48-60*
ISSN (Print) : 0013-466X
ISSN (Online) : xxxx-xxxx
DOI: 10.18311/JESCI/2025/51173

Electrochemical Evaluation of Metal-coated Steel Sheets in 3.5% NaCl Solution

M. Priyanka[1,3,$], Sukanta Badaik[2,3,#], Priyaranjan Mohapatra[1], Suryakanta Nayak[3] and Tapan Kumar Rout[3*]

[1]Department of Chemistry, Veer Surendra Sai University of Technology, Burla - 768018, Odisha, India

[2]Department of Chemistry, National Institute of Technology Jamshedpur, Jamshedpur - 831014, Jharkhand, India

[3]Surface Engineering Research Group, R&D Tata Steel Limited, Jamshedpur - 831001, Jharkhand, India

[$]Joint PhD scholar of Veer Surendra Sai University of Technology, Burla and Research & Development, Tata Steel Limited, Jamshedpur

[#]Joint PhD scholar of National Institute of Technology Jamshedpur and Research & Development, Tata Steel Limited, Jamshedpur

Abstract

Steel sheets are essential in numerous industries, offering versatile applications due to their strength, durability, and adaptability. These sheets are categorised based on composition, surface finish, and processing methods. Cold Rolled Close Annealed (CRCA) steel, mild steel, begins to corrode rapidly when exposed to open environments. Therefore, metallic coatings are often applied to protect it from corrosion. Commonly used metallic coatings include hot-dip galvanized iron (GI, ~8.4 µm), galvannealed (GA) steel (~8.4 µm), Galvalume (zinc with 55% aluminium, ~8.4 µm), and electroplated pure tin (Sn-coated steel, ~1.3 µm). Hot dip coated products are being used for automotive, construction, and general engineering segments whereas tinplate substrates are exclusively used for the food packaging segment. The study examines the anti-corrosion behaviour of different metallic coatings in 3.5% NaCl solution. A detailed characterisation study using SEM, XRD, and XRF with respect to coating composition, surface morphology, and phases is presented. Anticorrosion performance was characterized by potentiodynamic polarisation measurement, Electrochemical Impedance Spectroscopy (EIS), and accelerated Salt Spray Test (SST). It is observed that the surface finish, microstructural composition, and passivation layers significantly influence the corrosion behaviour of steel sheets in 3.5% NaCl solution. The corrosion resistance varies depending on these surface properties.

Keywords: Corrosion; EIS; Microstructure; Steel sheets; SST

1. Introduction

Steel is a widely utilized structural material known for its strength, ductility, and versatility, which makes it suitable for a broad range of engineering applications[1]. Fundamentally, steel is an alloy of iron containing a small proportion of carbon, typically less than 2%, which plays a crucial role in determining its mechanical properties, such as hardness, tensile strength, and toughness. The presence of carbon significantly enhances the strength and durability of the base metal by altering the microstructure, primarily through the formation of cementite and pearlite phases[2,3]. Among the numerous grades of steel, mild steel, also referred to as low-carbon or carbon steel, is one of the most used. It consists of more than 99% iron, with carbon content typically below 0.25%, along with manganese in similar low concentrations, and trace amounts of phosphorus and sulphur[4]. This composition yields a material that is easily

*Email: tapankumarrout@tatasteel.com

formable, weldable, and cost-effective, making it ideal for construction, automotive, and general manufacturing applications[5,6]. Steel sheets [CRCA (without any metallic coatings)] with specialized surface coatings such as GA, GI, Galvalume, and Sn-coated varieties, which play crucial role in various industries, including automotive, construction, and packaging. Each variant offers unique mechanical, chemical, and corrosion-resistance properties, determined by its production process and surface treatment. CRCA steel sheets are manufactured by cold rolling followed by a close annealing process, which enhances their formability and makes them suitable for a wide range of applications[7,8]. Research on CRCA sheets often focuses on their weldability, mechanical properties, and performance in hybrid joints. Mechanical testing and thermal analysis are commonly employed methodologies, revealing that optimal weld parameters can enhance joint performance and reduce undesirable effects like thinning or fracture during forming operations[9]. GA steel sheets are created by hot-dip galvanizing followed by annealing, producing a zinc-iron alloy coating that improves paint ability and corrosion resistance[10,11]. Studies show that while GA sheets perform well in neutral salt spray tests, both GA and CRCA sheets are susceptible to continuous corrosion if left unpainted[12]. GI sheets are steel substrates coated with pure zinc, primarily through hot-dip processes. Literature on GI sheets investigates the relationship between process parameters (such as coating thickness and bath composition) and final properties like formability, ductility, and fracture resistance[13,14]. Galvalume sheets are coated with a zinc–aluminium alloy that provides both sacrificial protection (from zinc) and barrier protection (from aluminium). During corrosion, aluminium forms a stable oxide film such as Al_2O_3, which enhances protection[15]. Zinc and aluminium forms together to provide superior corrosion protection for steel compared to the traditional galvanized steel. The zinc-aluminium alloy coating offers both long-term corrosion resistance and galvanic protection, especially at cut edges. At cut edges, zinc in galvalume provides sacrificial protection, minimizing rust staining, while the aluminium helps to prevent the corrosion from spreading. In Galvalume, zinc also contributes to the "self-mending action", where zinc dissolves out, and the aluminium oxides fill in those spaces. Studies comparing galvalume to GI sheets identify superior corrosion resistance and formability in galvalume, making it especially suitable for roofing and cladding where corrosion resistance is crucial. Mechanical and tribological tests reveal that the aluminium content provides ductility and improved behaviour under wear conditions[16]. Sn-coated steel is most used in packaging, such as food and beverage cans, due to its excellent corrosion resistance and formability[17,18]. Tin coating also enhances lubricity, which is beneficial in forming operations[19]. The commonly used steel sheets are CRCA, GA, GI, Galvalume, and Sn-coated steel, which are primarily based on low-carbon steel, typically comprising 0.03–0.10% carbon (C), 0.25–0.50% manganese (Mn), with phosphorus (P) and sulphur (S) each below 0.035%, and the balance being iron (Fe). CRCA steel is uncoated and retains this base composition[20]. GA (Galvannealed) steel is coated with a zinc-iron alloy layer, typically containing about 90% zinc (Zn) and 10% iron (Fe) formed by diffusion during annealing. GI steel is hot dip coated with nearly pure zinc, typically around 99.5% Zn, with small additions of aluminium (~0.2%) and trace elements like lead (Pb), or antimony (Sb) for coating control. Galvalume steel features a hot-dip coating composed of approximately 55% aluminium (Al), 43.5% zinc (Zn), and 1.5% silicon (Si), providing enhanced corrosion resistance. Sn-coated steel is coated with a very thin electrolytic layer of tin (Sn) in the range of 0.1–1.0%, while the substrate remains the same low-carbon steel. Several recent studies have focused on the analysis of anticorrosion behaviour of steel sheets, aiming to enhance durability and resistance in aggressive environments[21-25]. These differences in surface composition significantly impact corrosion resistance, formability, and application suitability. However, despite their respective advantages, important research gaps remain for each steel type. One of them is the need for more comprehensive long-term corrosion studies. In this work, we have done characterisations performed characterizations like such as FTIR, Raman, and XRD to determine the presence of various functional groups and phases present in the steel sheets. Anticorrosion studies, including Salt Spray Test (SST) in a 5% NaCl solution, Electrochemical Impedance Spectroscopy (EIS), and potentiodynamic polarization (Tafel analysis), were conducted to evaluate the corrosion resistance of the steel sheets. Finally, the chemical composition, microstructural and wettability properties were obtained through SEM-EDS, X-Ray Fluorescence (XRF) spectrometer, and contact angle studies. Anti-corrosion analysis of steel sheets is crucial for ensuring their longevity and reliability in various applications. By evaluating the corrosion resistance of different steel types, we can identify the most

suitable materials for specific environments, optimize protective measures, and ultimately prevent costly failures and replacements.

2. Materials and Methods

1.1. Sample Preparation

Samples were collected and cut into coupon size (10 cm x 4 cm) for the study. The samples were degreased using an alkali solution (Rhidoline 1352B) and then rinsed with tap water and distilled water as well. Then dried them through a hot air dryer.

1.2. Characterization

Fourier Transform Infrared (FTIR) spectroscopy is used for the detection of functional groups. The test was carried out using Bruker Vertex 80 V with a range of 400 to 4000 cm^{-1} in ATR mode. Raman microscopy is used to record Raman spectra of coated substrate for 10 seconds of exposure time within the range of 100-3204 (centre-1111) Raman shift/cm^{-1} at a continuous scan rate to identify the chemical bond formed on the coated substrate. Scanning electron microscope gives information about the sample, such as chemical composition, external morphology, orientation, and crystalline structure of the specimen. Energy Dispersive X-ray (EDX) spectroscopy is used for the elemental composition of different steel substrates used in this study and it is conjugated with SEM instrument (Apreo S). PANlytical Xpert Pro diffractometer is used for analysing the structure of crystalline materials. An X-ray Fluorescence, a non-destructive analytical technique used for the determination of the elemental composition of materials through Shimadzu EDX-7200. Electrochemical Impedance Spectroscopy (EIS) measures the impedance of an electrochemical system across a range of frequencies. This technique helps characterize the system's resistance, capacitance, and inductive properties. The experiment was carried out using a Gamry Potentiostat. Tafel Analysis is a method in electrochemistry used to analyse the kinetics of electrochemical reactions, particularly corrosion processes. This technique was used to determine key parameters like the exchange current density and the Tafel slopes, which provided insights into reaction mechanisms and the rate of electron transfer. Salt spray test was carried out to evaluate the corrosion resistance of materials and surface coatings (metallic-primary coatings). The wettability of steel sheets was verified by the iDS Contact Angle System using DM water as the testing liquid. The surface roughness was measured by CLSM (Confocal Laser Scanning Microscope) of model no 2F44045 for high-resolution imaging of surface topography, including surface roughness.

3. Results and Discussion

3.1. Fourier Transform Infrared Spectroscopy (FTIR) study

The FTIR spectra of CRCA, GA, GI, galvalume, and Sn-coated were recorded across the wavenumber range of 400–4000 cm^{-1} and shown in Fig. 1. Due to the metallic nature of the samples, low transmittance was observed. Each sample exhibits subtle differences in transmittance across the wavenumber range, indicating slight variations in surface chemistry or coating composition. The C=N peak was observed at 1640 cm^{-1} for GA and GI[26]. Additionally, the -OH functional groups at ~3450 cm^{-1} were observed for CRCA, GA, GI, and Galvalume[27]. Apart from the mentioned peaks, no other functional groups were found in all substrates, making them less reactive.

3.2. Raman Spectroscopy Study

The Raman spectra of CRCA, GA, GI, Galvalume, and Sn-coated steel sheets exhibit several distinct peaks corresponding to characteristic vibrational modes of their surface oxide compositions. The corresponding spectra are presented in Fig. 2. In the case of CRCA (Fig. 2a), prominent Raman peaks were observed at 1335 cm^{-1} and 1605 cm^{-1}, corresponding to the vibrational modes of

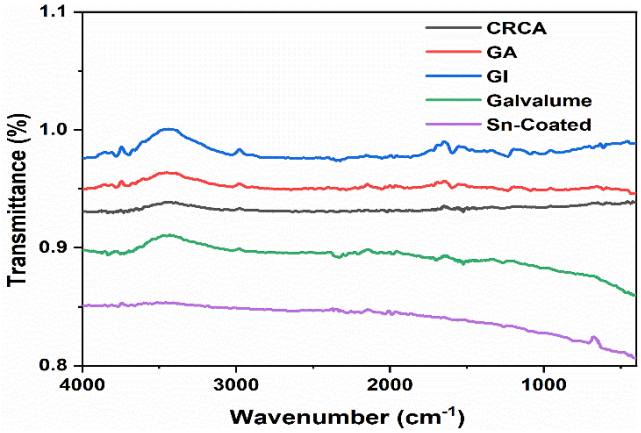


Fig. 1. FTIR Spectra of different steel substrates (CRCA, GA, GI, Galvalume, and Sn-coated steel).

Fe_2O_3 and either Fe_3O_4 or FeOOH, respectively[28]. These features indicate the presence of mixed iron oxide phases on the surface. For GA (Fig. 2b), a peak at 811 cm^{-1} was identified, which can be attributed to Zn-O or Fe-O vibrational modes[29]. These modes likely arise from complex surface oxides formed during the galvannealing process. The GI (Fig. 2c) sample exhibits a strong and broad peak centered at 1334 cm^{-1}, characteristic of the D-band in carbonaceous materials, suggesting the presence of surface carbon contamination or residual organic compounds. Additionally, multiple peaks below 800 cm^{-1} are evident, which are typically associated with Zn-O vibrational modes, indicative of surface oxidation of zinc during or after the galvanization process[30]. In the case of Galvalume (Fig. 2d), the Raman spectrum is dominated by a sharp peak at approximately 515 cm^{-1}, which corresponds to Al-O vibrational modes[31]. The absence of significant carbon or iron oxide signals suggests a surface predominantly composed of aluminium oxide, reflecting a chemically stable and protective oxide layer. For the Sn-coated steel sheet (Fig. 2e), a distinct peak at 126 cm^{-1} was observed, likely corresponding to Sn-O lattice vibrations[32]. Additionally, a sharp and intense peak at 145 cm^{-1} was detected, which is the characteristic of the Raman-active modes of crystalline SnO_2. The intensity and definition of these peaks suggest the formation of a well-crystallized SnO_2 surface layer. These spectral features provide critical insights into the chemical nature and stability of the oxide layers formed on the various metallic coated steel substrates.

3.3. Scanning Electron Microscope (SEM)

A scanning electron microscope was used to understand the surface morphology of all samples. The obtained surface and cross-sectional microstructure were shown in (Fig. 3a-j), and EDX analysis (Fig. 3k-o) confirmed the various elements present in the steel substrates. In CRCA (Fig. 3a), the surface appears to have some irregularities and roughness, possibly due to rolling and mechanical deformations. The presence of grain boundaries and fine microstructure suggests a heat treatment effect due to annealing[33]. The cross-sectional images reveal the internal microstructure, including grain size and phase distribution[34].

In the case of galvannealed (GA) steel (Fig. 3b), the surface appears rough and irregular, with distinct granular-like structures. The cross-sectional micrograph illustrates a well-developed structure characterized by compact grains and crystallized regions, which reflect the solidification behavior of the surface coating. The upper rough region visible in the image denotes an interface between the steel substrate and the protective zinc-iron alloy layer, formed during the galvannealing process[27,35]. The galvanized (GI) steel surface (Fig. 3c) demonstrates a

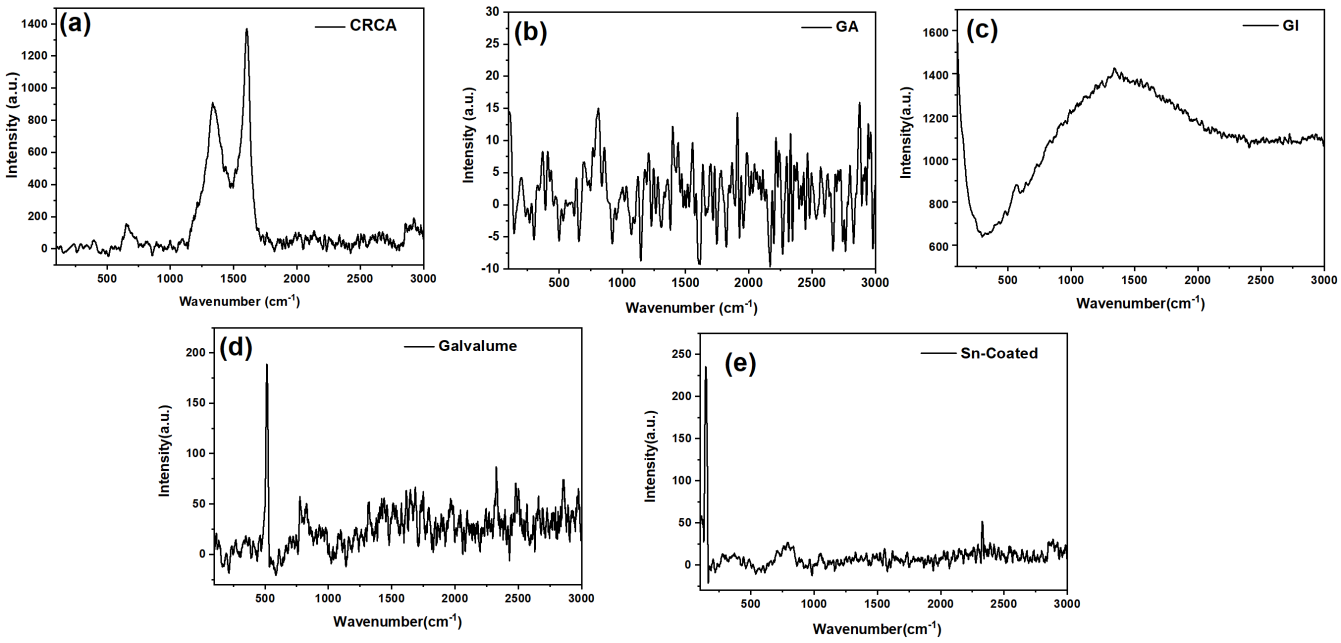


Fig. 2. Raman Spectra of **(a)** CRCA, **(b)** GA, **(c)** GI, **(d)** Galvalume, and **(e)** Sn-Coated sheets.

rough morphology with discernible grain boundaries and surface cracks, typical of the zinc coating applied during hot-dip galvanization. These surface features correspond to the formation of zinc crystals or spangles. The cross-sectional image (Fig. 3h) highlights the polygonal grain structure of the zinc layer, with relatively uniform grain size and shape, indicative of good Galvanization quality[36]. The surface microstructure of galvalume steel (Fig. 3d) is characterized by a distinct dendritic or rod-like morphology, reflecting the Al-Zn eutectic microstructure that develops during solidification. This dual-phase structure consists of Al-rich dendrites interspersed with Zn-rich regions. The cross-sectional view (Fig. 3i) reveals a fine-grained, homogeneous coating layer, highlighting well-defined grain boundary networks[37]. The presence of bright lines at grain interfaces suggests Al-Zn crystal boundaries or diffusion zones, which are typical of high-quality Galvalume coatings. The surface microstructure of

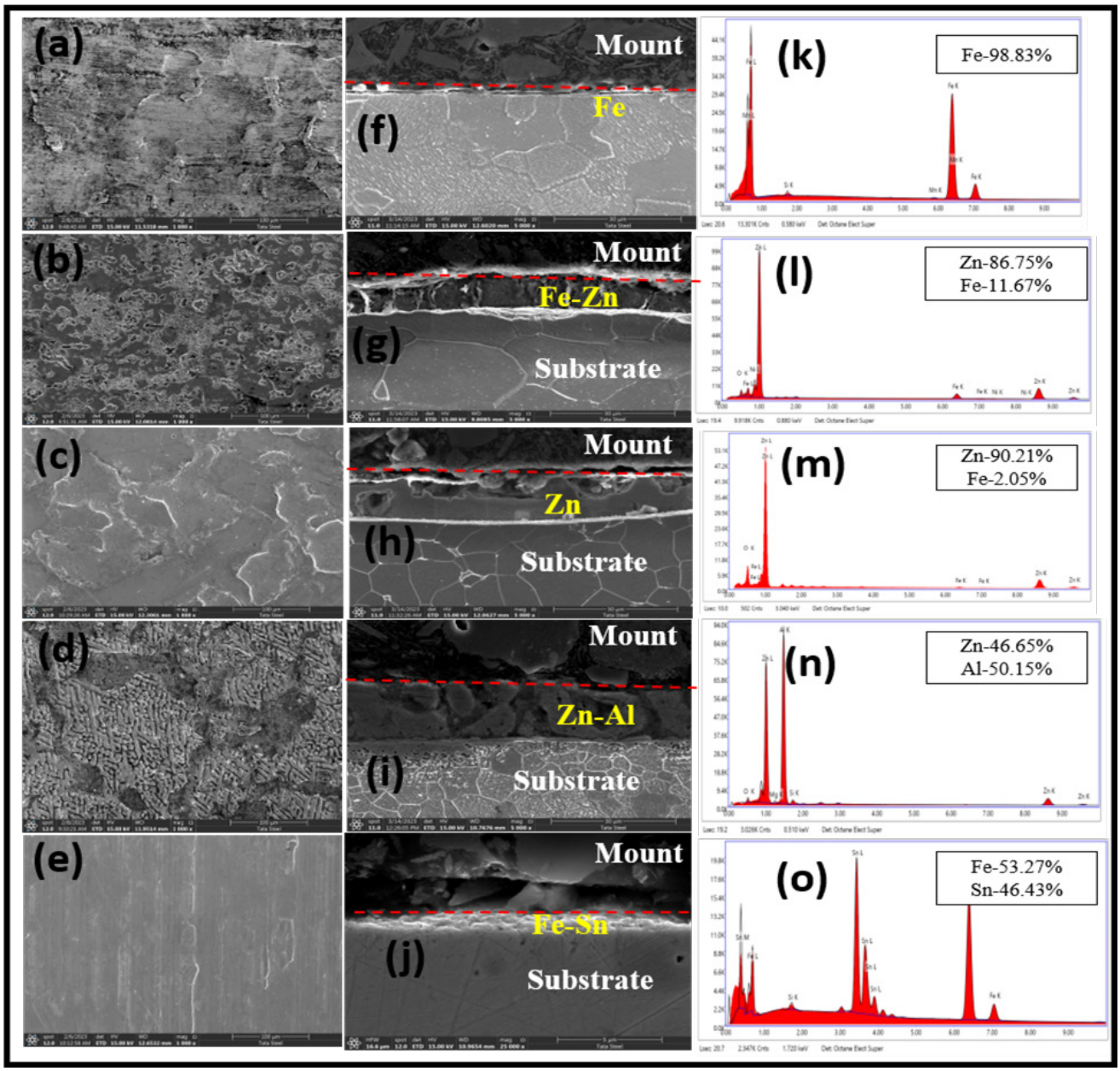


Fig. 3. SEM images showing (a-e) surface morphology, (f-j) cross-section, and (k-o) EDS spectra of surface for CRCA, GA, GI, Galvalume, Sn-Coated sheets, respectively.

tinplate (Fig. 3e), which consists of a thin layer of metallic tin electroplated onto low-carbon steel, exhibits a smooth and continuous morphology[38]. The cross-section image showed the formation of the smooth Fe-Sn intermetallic layer, enhancing its anticorrosion property.

Complementary Energy-Dispersive X-ray Spectroscopy (EDS) was performed to analyze the interface elemental composition for each substrate. In CRCA, prominent peaks for Fe and Mn (Fig. 3k) validated the presence of iron and manganese. GA and GI samples showed distinct peaks for Fe, Zn, and O, indicating the presence of zinc coatings and possible surface oxidation. The Galvalume coating revealed characteristic peaks for Al, Zn, Si, and O, confirming the dual-phase Al-Zn composition. Lastly, the Sn-coated samples exhibited clear peaks for Fe, Sn, and Si, verifying the tinplate composition.

3.4. X-Ray Diffraction (XRD) Analysis

X-Ray Diffraction (XRD) analysis was conducted to identify the various phases present in the steel sheets. The resulting diffraction patterns, which provide insights into the crystalline structure and phase composition, are presented in Fig. 4.

For the CRCA (Fig. 4a) steel, prominent diffraction peaks were observed at 2θ values of 44.6° (111), 64.6° (020), 82.7° (121), and 78.2° (055). These peaks matched with standard JCPDS file nos. 96-901-3476 and 96-901-2712 corresponding to iron (Fe), and 96-151-2521 for manganese (Mn), confirming the ferritic phase of the steel substrate[39]. In the case of the GA (fig.4b), diffraction peaks appeared at 2θ values of 36.6° (311), 37.4° (−112), 41.2° (401), 42.5° (−421), 42.8° (202), 47.9° (421), 65.1° (−423), and 74.0° (−802), corresponding to iron-zinc alloy phases as per JCPDS file no. 96-201-0724. Additional peaks at 44.5° (011) and 82.3° (112) matched with the JCPDS file no. 96-901-3474 (Fe) and 96-901-2436 (Zn), confirming the presence of both elemental iron and zinc in the microstructure[40]. For the GI (Fig. 4c), the XRD pattern exhibited peaks at 2θ values of 36.1° (002), 38.9° (100), 43.2° (101), 54.1° (102), 70.0° (013), and 82.4° (121). These peaks matched well with JCPDS file numbers 96-901-1600 (Zn), 96-900-8523 (Zn), and 96-901-3473 (Fe), indicating a typical zinc-coated steel surface. The Galvalume (Fig. 4d) showed diffraction peaks at 36.3° (002), 43.2° (101), 54.3° (102), 82.3° (112), and 86.5° (201), which corresponded to zinc phases as per JCPDS file nos. 96-901-2436 and 96-900-8523. Additionally, peaks at 38.6° (111), 44.9° (020), 65.3° (022), and 78.5° (131) were matched to aluminium phases (JCPDS file no. 96-150-2690), indicating the dual-phase Al-Zn structure typical of Galvalume[41]. A minor peak at 70.3° (062) was identified as zinc-iron oxide, as per the JCPDS file number. 96-200-9104. For the Sn-coated

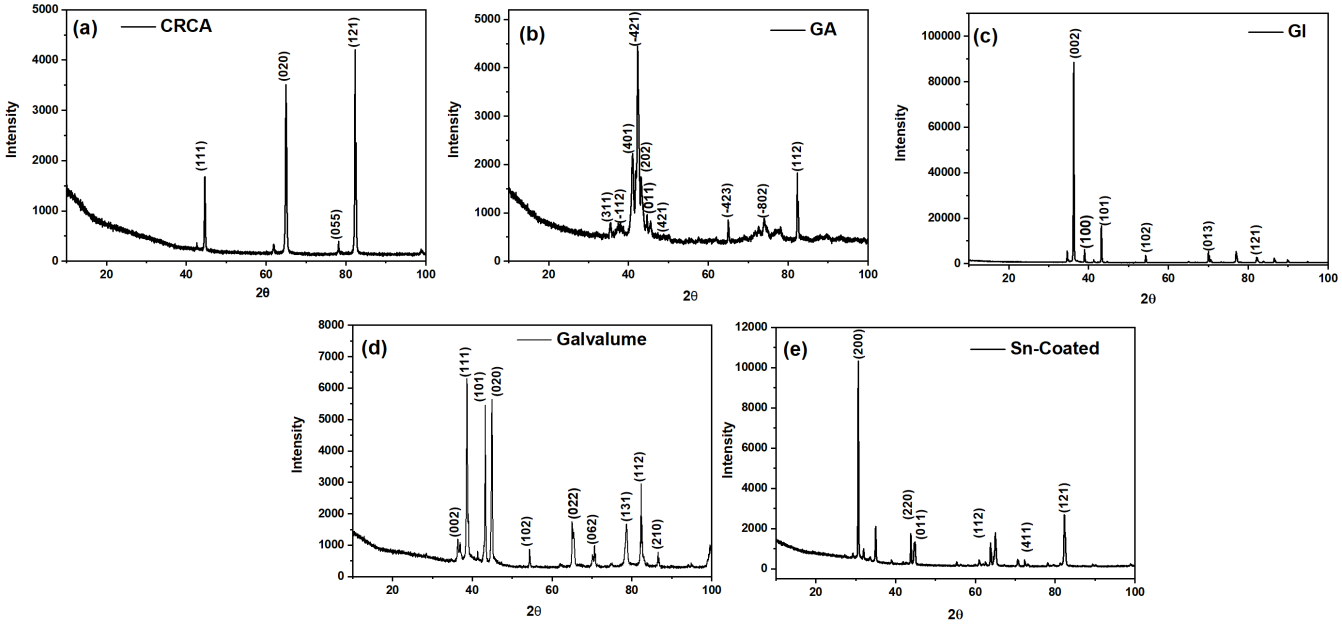


Fig. 4. XRD graphs of **(a)** CRCA, **(b)** GA, **(c)** GI, **(d)** Galvalume and **(e)** Sn-Coated steel sheets.

Table 1. Elemental composition of all samples found in XRF Spectroscopy

SAMPLE NAME	Fe (%)	Zn (%)	Mn (%)	Cr (%)	Ca (%)	Al (%)	Si (%)	Sn (%)	Sc (%)	Ge (%)
CRCA	99.819		0.117	0.064	-	-	-	-	-	-
GA	37.999	61.898	0.041	-	0.062	-	-	-	-	-
GI	20.185	79.768	0.047	-	-	-	-	-	-	-
Galvalume	27.424	26.492	0.062	-	-	45.286	0.736	-	-	-
Sn-Coated	98.357	-	-	0.062	-	-	0.662	0.443	0.047	0.023

sample (Fig. 4e), diffraction peaks were observed at 2θ values of 30.6° (200), 43.8° (220), 62.5° (112), and 73.1° (411), which aligned with the JCPDS file no. 96-704-0218 (Sn), confirming the presence of tin[42]. Additional peaks at 44.9° (011) and 82.3° (121) matched with the JCPDS file nos. 96-900-6588 (Fe), indicating the underlying steel substrate.

3.5. Elemental Analysis by X-Ray Fluorescence (XRF) Spectrometer

The XRF analysis Table 1, provided the elemental composition of all samples. CRCA is nearly pure Fe (99.819%) and minor traces of Mn (0.117%) and Cr (0.064%). GA is predominantly composed of Zn (61.898%) and Fe (37.999%) and minor amounts of Mn (0.041%), Cr (0.062%), and Ca (0.062%). In contrast, GI contains a higher percentage of Zn (79.768%) and Fe (20.185%) with traces of Mn (0.047%). Both are Fe-Zn alloys, but GI has a higher Zn percentage, making it more resistant to corrosion compared to GA. Similarly, Galvalume has balanced Fe (27.424%) and Zn (26.492%) content, high Al content (45.286%) and minor amounts of Mn (0.062%) and Sn (0.736%). Although a thin Sn coating (0.443%) likely provides a protective layer for Fe, enhancing corrosion resistance. The anticorrosion property of the above substrates was verified by potentiodynamic polarization study.

3.6. Electrochemical Studies

3.6.1. Polarisation Study of Different Substrates using Potentiodynamic Polarization Measurement

Electrochemical characterizations such as potentiodynamic polarization (Tafel test) and Electrochemical Impedance Spectroscopy (EIS) are utilised to understand the anticorrosion behaviour of different steel substrates. The obtained Tafel plot is shown in Fig. 5a, and the corresponding fitted parameters, including anodic Tafel slope (β_a), cathodic Tafel slope (β_c), corrosion potential (E_{corr}), and corrosion current density (I_{corr}) are detailed values are given in Table 2.

Table 2. Fitted Tafel parameter for all substrates

Sample ID	βa (V/ decade)	βc (V/ decade)	I_{corr}(nA)	E_{corr}(V)
CRCA	2.226	0.243	203	-0.415
GA	0.073	0.512	2410	-0.915
GI	0.001	0.037	7590	-1.310
Galvalume	0.179	0.094	14700	-1.320
Sn-Coated	0.083	0.339	495	-0.553

The obtained E_{corr} values for CRCA, GA, GI, Galvalume and Sn-Coated sheets are -0.415V, -0.915V, -1.310V, -1.320V, and -0.553V, respectively. The highest E_{corr} value was observed by CRCA, whereas the lowest corrosion potential was obtained by galvalume. As we know, zinc potential is higher than iron, so it is more reactive and tends to lose electrons and undergo oxidation[43]. The presence of zinc in GA, GI, and Galvalume formed a passivating zone on the anodic region. On the other hand, the presence of high iron in CRCA (99.81%) sheet makes them more prone to oxidation. But in Sn-coated substrate, the thin layer of tin coating acts as a sacrificial anode, showing E_{corr}, -0.553V. Additionally, the lowest corrosion current density (I_{corr}) was observed for Sn-coated (495 nA), signifying the least oxidation nature among all substrates.

3.6.2. Electrochemical Impedance Spectroscopy (EIS) Study

Electrochemical Impedance Spectroscopy (EIS) is a powerful and non-destructive technique widely used to investigate the electrochemical properties of materials and interfaces. Here, Randles' equivalent circuit was used

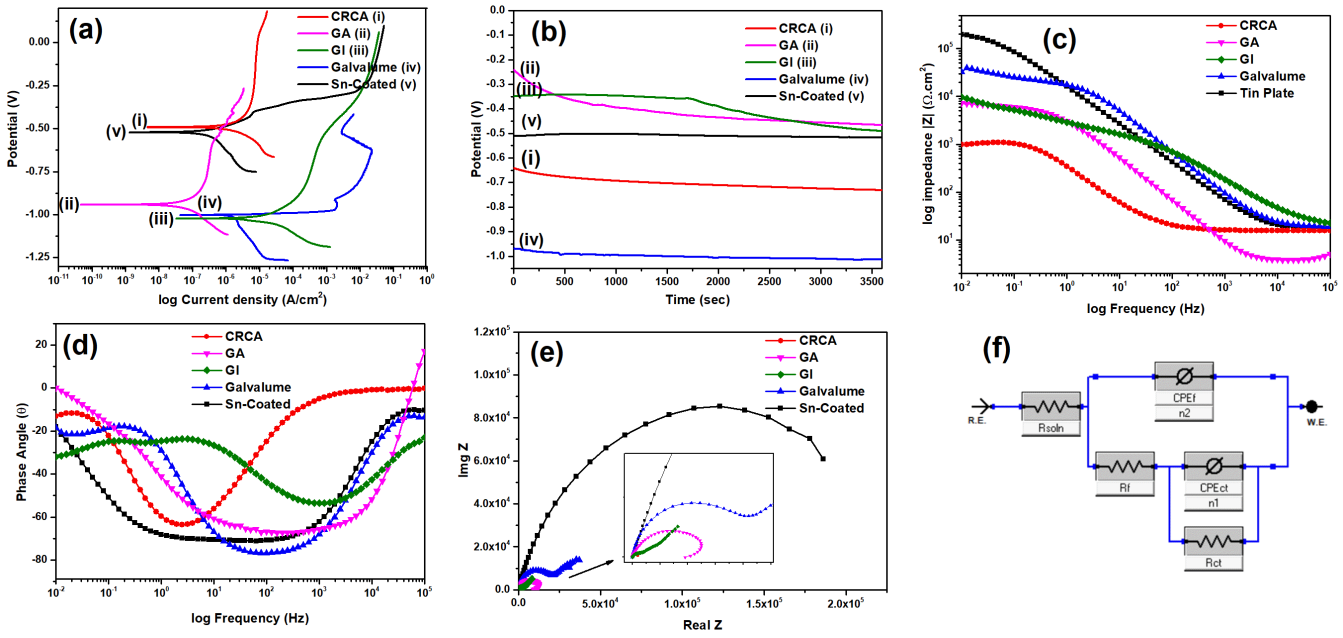


Fig. 5. **(a, b)** Tafel and open circuit potential (OCP) plots, **(c)** Bode impedance, **(d)** Bode phase angle, and € Nyquist plot of CRCA, GA, GI, Galvalume, and Sn-coated in 3.5% NaCl solution, and **(f)** Randles circuit used for fitting the EIS data.

Table 3. Electrochemical impedance parameters derived from EIS fitting for various coated steel substrates in 3.5% NaCl medium

Sample ID	R_{soln} ($\Omega.cm^2$)	R_{ct} ($\Omega.cm^2$)	R_f ($\Omega.cm^2$)	CPE_{ct} (S^*s^a)	n_1	CPE_f (S^*s^a)	n_2	Total Resistance (R_t) = R_{ct}+ R_f ($\Omega.cm^2$)
CRCA	15.75		1150			0.000585	0.828	1150
GA	4.67	12700	57.94	0.0000281	0.695	0.00000225	0.792	12700
GI	17.06	12400	1520	0.000301	0.357	0.0000126	0.693	14000
Galvalume	18.52	68900	20100	0.000154	0.56	0.00000485	0.884	89000
Sn coated	16.68	236000	4390	0.00000448	0.663	0.00000993	0.842	240000

to fit the obtained graphs. A Constant Phase Element (CPE) has been used instead of a pure capacitor, and n1 and n2 are taken as exponents. The parameters like R_{soln}, R_{ct} (charge transfer resistance), R_f (resistance of steel sheet) and CPE_{ct} (the capacitance associated with the charge transfer phenomenon), CPE_f (capacitance of the coating), total resistance (R_t) = R_{ct}+ R_f were calculated, and detailed values are given in Table 3.

The obtained Bode, Nyquist plots and the Randles equivalent circuit used for fitting of coated samples are shown in Fig. 5c-f. The obtained total resistance for CRCA, GA, GI, Galvalume, and Sn-Coated substrates are 1.15×10^3 $\Omega.cm^2$, $1.27\times10^4\Omega.cm^2$, 1.24×10^4 $\Omega.cm^2$, 8.90×10^4 $\Omega.cm^2$, and 2.40×10^5 $\Omega.cm^5$ respectively. The Sn-coated sheet exhibited the highest impedance, indicating superior barrier properties. Conversely, the CRCA sheet showed the lowest impedance, reflecting poor corrosion resistance. The observed phase angle at 10Hz for CRCA, GA, GI, Galvalume, and Sn-Coated substrates are -58°, -62°, -33°, -73°, and -70°, respectively. The shifting of the phase angle towards -90° suggests that the material is capacitive in nature, having a stable protective layer. This indicated that galvalume and Sn-coated sheets have a stable protective layer of Al and Sn, which can give some advancement in anticorrosion properties compared to other substrates[44,45]. In the Nyquist plot, we know that the bigger the semicircle, the better the anticorrosion property[46]. The biggest semicircle was formed by Sn-coated substrate, whereas the smallest semicircle was formed by CRCA (Fig. 5e). Additionally,

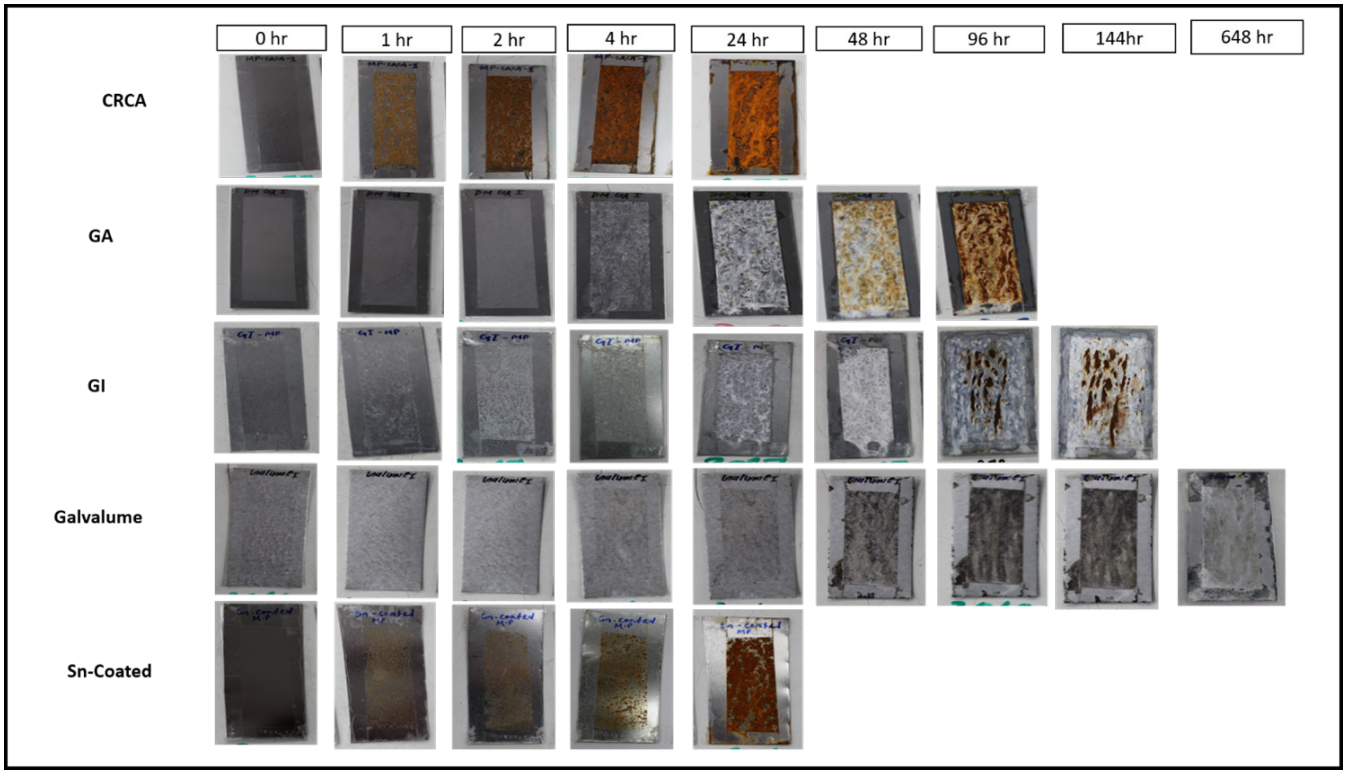


Fig. 6. Photographs of the surface of exposed samples at various corrosion exposure times.

the 45° tail observed in the Nyquist plots of GA and GI indicates Warburg impedance, suggesting ongoing water diffusion[46,47].

3.7. Accelerated Corrosion Study by using Salt Spray Test Chamber

Salt Spray Test (SST) is a standardized test as per ASTM B117 used to assess a material's protective behaviour against corrosion under accelerated environmental conditions (a salt fog environment -5% NaCl solution at 35°C and RH = ~95%). The samples were subjected to an SST chamber, and the obtained images are shown in Fig. 6.

Among all tested substrates, Cold Rolled Close Annealed (CRCA) steel exhibited the most rapid corrosion response. Red rust formation, an indicator of direct iron oxidation, was evident within the first hour of exposure. Corrosion aggressively progressed, reaching approximately 50% surface coverage by 2 hours, and culminating in complete rust coverage at just 4 hours. The rapid onset and full development of red rust underscore CRCA's poor resistance to chloride-induced corrosion. GA demonstrated improved initial corrosion resistance due to the zinc-iron alloy layer. After 2 hours of exposure, localized blistering and white rust characteristic of zinc oxidation began to appear. The sample exhibited 100% white rust coverage in 24 hours. Upon extended exposure (up to 96 hours), the zinc barrier was depleted, allowing red rust to emerge from the underlying steel, marking complete failure of the coating by the fourth day. GI followed a similar trend, with corrosion initiation noticeable at 1 hour. The sample showed complete white rust coverage within 24 hours, indicating rapid depletion of the protective zinc layer. By 96 hours, over 50% red rust had developed on the corroding substrate. Galvalume, an aluminium-zinc alloy-coated steel, initially resisted red rust formation. Instead, early signs of corrosion manifested as white rust at 1 hour. By 24 hours, as the zinc component oxidized, dark spots emerged, attributed to aluminium oxide or "black rust". These spots proliferated, leading to full-surface corrosion coverage by 96 hours. The transition from white to black rust reflects the sequential exhaustion of zinc and exposure of the aluminium layer[48]. In contrast, the tin-coated steel sample exhibited red rust onset within the first hour, similar to CRCA, with corrosion coverage intensifying over time. The surface was entirely rusted in 24 hours, indicating

the limited protective nature of the tin layer under salt spray conditions. The observed corrosion products are white rust (zinc oxides), red rust (iron oxides), and black rust (aluminium oxides), corresponded directly with the elemental composition of each coating[45]. These observations were in strong agreement with EIS results, further validating the SST findings.

3.8. Contact Angle Measurements

The contact angle data demonstrate how surface chemistry and texture affect wettability. The obtained contact angle images are shown in Fig. 7.

The measured contact angles for CRCA, GA, GI, Galvalume, and Sn-coated substrates were 63.85°, 68.8°, 86.75°, 83.2°, and 94.75°, respectively. CRCA, GA, GI, and galvalume, these surfaces appear to have moderate contact angles, suggesting they are close towards hydrophilic. The zinc coating provides a hydrophobic surface, often enhanced by surface texture. Galvalume has a high contact angle, possibly the highest among all. The Al-Zn alloy coating on galvalume offers a smoother and more chemically inert surface, resulting in strong hydrophobic behaviour. Sn-coated surface shows a lower contact angle, indicating it is more hydrophilic compared to others. The higher contact angle suggests good water repellence [49], beneficial for corrosion resistance.

3.9. Surface Roughness

The surface roughness was measured by CLSM (Confocal Laser Scanning Microscope), and the obtained images are shown in Fig. 8. The roughness was measured at three different places for each sample, and average values were taken. The exhibited data for CRCA, GA, GI, galvalume and Sn-Coated are 1.125 µm, 1.858 µm, 1.787 µm, 0.339 µm and 0.443 µm, respectively. GA showed the highest roughness (1.858 µm), whereas galvalume showed the lowest roughness (0.339 µm). In the case of GA, the formation of hard, irregular Fe-Zn intermetallic phases

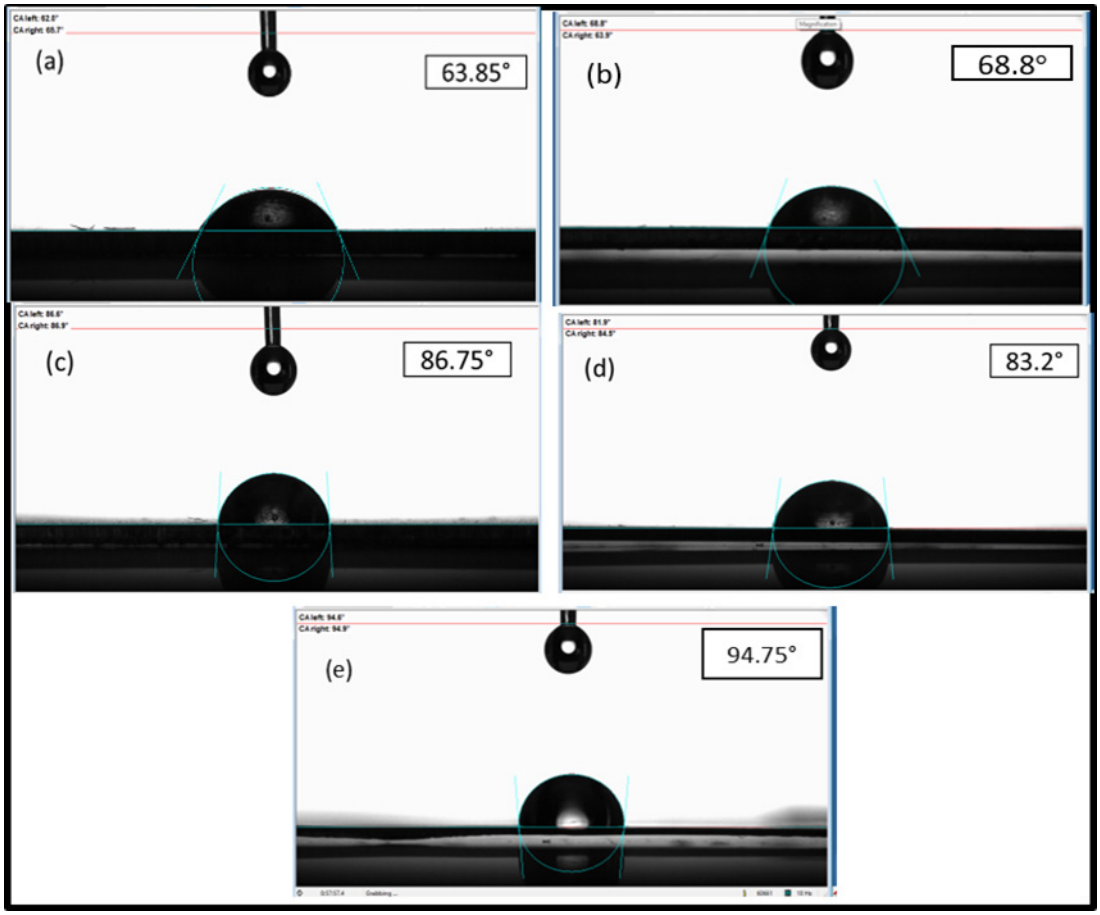


Fig. 7. Contact angle images for **(a)** CRCA, **(b)** GA, **(c)** GI, **(d)** Galvalume, and **(e)** Sn-Coated steel sheets.

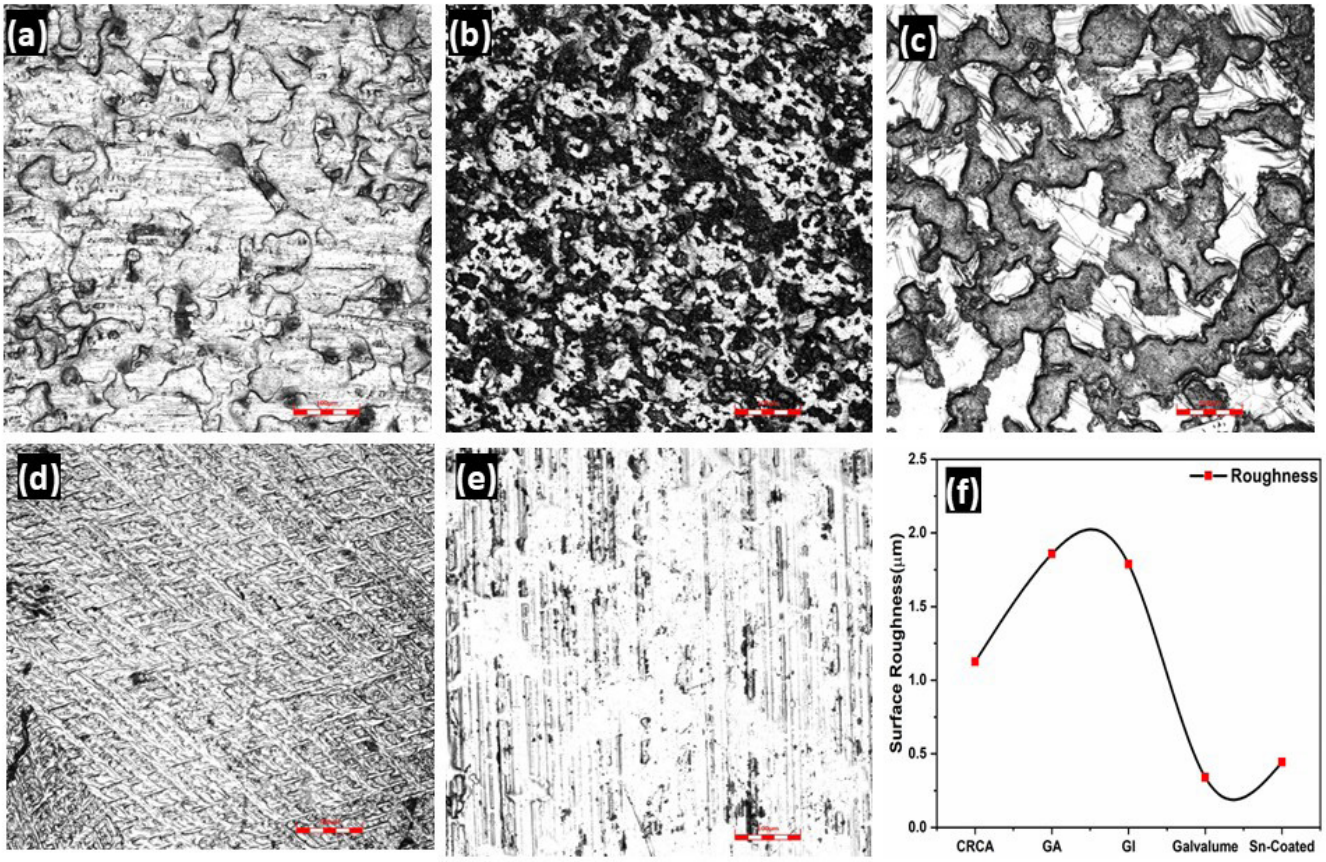


Fig. 8. CLSM images of **(a)** CRCA, **(b)** GA, **(c)** GI, **(d)** Galvalume, **(e)** Sn-Coated and **(f)** Surface roughness graph.

during the annealing process leads to a rough, non-uniform surface compared to GI or uncoated CRCA steel.

4. Conclusions

In this study, we employed various characterization techniques to understand the composition, structure, morphology, and anticorrosion behaviour of different metallic coatings on mild steel substrates. Metallic coatings such as hot-dipped galvanised (GA and GI) and aluminium in Galvalume coatings provide enhanced protection against corrosion, primarily by acting as effective barriers and sacrificial layers. The Salt Spray Test (SST) results were in strong agreement with the electrochemical measurements, supporting the observed trends in corrosion resistance. Among the tested materials, the Sn-coated steel exhibited superior Corrosion Resistance Compared to Cold-Rolled Close-Annealed (CRCA) mild steel. Contact angle measurements indicated that all metallic coating of tin on mild steel exhibited more water repellent behaviour than CRCA. Furthermore, Electrochemical Impedance Spectroscopy (EIS) revealed that the Sn-coated steel had the highest impedance (>10^5 Ω·cm^2), indicating the best barrier properties. In contrast, CRCA showed the lowest impedance (~10^3 Ω·cm^2), confirming its inferior corrosion protection.

5. Acknowledgements

The authors gratefully acknowledge the support of the management of TATA Steel Pvt. Ltd. for granting permission to publish this work. We also extend our sincere thanks to the laboratory staff (Ms. Puja Kumari, Ms. Puspanjali Mohanta, and Mr. Abhay Kumar) for their valuable assistance during the experimental and characterization processes. We further appreciate the contributions of our research colleagues for their consistent support throughout the study.

6. References

1. Gedge G. Structural uses of stainless steel - buildings and civil engineering. J. Constr. Steel Res. 2008; 64, 1194-1198. https://doi.org/10.1016/j.jcsr.2008.05.006.
2. Dwivedi D, Lepková K, Becker T. Carbon steel corrosion: a review of key surface properties and characterization methods. RSC Adv. 2017; 7, 4580-4610. https://doi.org/10.1039/C6RA25094G.

3. Abdullah M., Muttalib MA, Alam ZF, Hossain MM, Ahsan Z. Effects of temperature and water pressure on mild steel strength: A comparative study. Results in Surfaces and Interfaces. 2024; 17, 100333. https://doi.org/10.1016/j.rsurfi.2024.100328.
4. Rodionova IG, Feoktistova MV, Baklanova ON, Amezhnov AV, D'yakonov DL. Effect of Chemical Composition and Microstructure Parameters on Carbon and Low-Alloy Steel Corrosion Resistance. Metallurgist. 2018; 61, 770-776. https://doi.org/10.1007/s11015-018-0562-9.
5. Singh MK. Application of steel in automotive industry. Int. J. Emerg. Technol. Adv. Eng. 2016; 6, 246-253. www.ijetae.com.
6. Baddoo NR, Stainless steel in construction: A review of research, applications, challenges and opportunities. J. Constr. Steel Res. 2008; 64, 1199-1206. https://doi.org/10.1016/j.jcsr.2008.07.011
7. Mohanty I,Datta S, Bhattacharjee D. Composition-processing-property correlation of cold-rolled if steel sheets using neural network. Mater. Manuf. Process. 2009; 24, 100-105. https://doi.org/10.1080/10426910802543947
8. Das S, Narayanan GR. Lap shear fracture prediction of friction stir spot welds between AA6063-T6 and CRCA/IS-513 sheets. Proc. Inst. Mech. Eng. Part E J. Process Mech. Eng. 2025. https://doi.org/10.1177/09544089251335077
9. Prashanthkumar VK, Venkataram N, Mahesh NS, Kumarswami. Process Parameter Selection for Resistance Spot Welding through Thermal Analysis of 2mm CRCA Sheets. Procedia Mater. Sci. 2014; 5, 369-378. https://doi.org/10.1016/j.mspro.2014.07.279
10. Shukla SK, Saha BB, Triathi BD, Avtar R. Effect of Process Parameters on the Structure and Properties of Galvanized Sheets. J. Mater. Eng. Perform. 2010; 19, 650-655. https://doi.org/10.1007/s11665-009-9527-2.
11. Hashiguchi K, Yasuda A, Hanazawa T, Ohori M, Ichida T. Galvannealed sheet steel with excellent press formability. Rev. Met. Paris. 1989; 87(3), 277-284. https://doi.org/10.1051/metal/199087030277
12. Bandyopadhyay N, Jha G, Singh AK, Rout TK, Rani N. Corrosion behaviour of galvannealed steel sheet. Surf. Coatings Technol., 2006; 200, 4312-4319. https://doi.org/10.1016/j.surfcoat.2005.02.153
13. Safaeirad M, Toroghinejad MR, Ashrafizadeh F. Effect of microstructure and texture on formability and mechanical properties of hot-dip galvanized steel sheets. J. Mater. Process. Technol. 2008; 196, 205-212. https://doi.org/10.1016/j.jmatprotec.2007.05.035
14. Gupta AK, Kumar DR. Formability of galvanized interstitial-free steel sheets. J. Mater. Process. Technol. 2006; 172, 225-237. https://doi.org/10.1016/j.jmatprotec.2005.10.016
15. Yadav M, Saha JK, Ghosh SK. Evaluation of mechanical and tribological behavior of galvanized, galvalume and polyurethane-coated steel sheets. Eng. Res. Express, 2023; 5, 015064. https://doi.org/10.1088/2631-8695/acc1c3.
16. Coni N, Gipiela ML, D'Oliveira ASCM, Marcondes PVP. Study of the mechanical properties of the hot dip galvanized steel and galvalume®. J. Brazilian Soc. Mech. Sci. Eng. 2009; 31, 319-326. https://doi.org/10.1590/S1678-58782009000400006.
17. Dean RR, Thwaites CJ. Tinplate and Tin Coating Technology. The Journal of The Minerals, Metals & Materials Society (TMS). 1987; 39, 42-45. https://doi.org/10.1007/BF03258609
18. Dey S, Agrawal MK. Tinplate as a Sustainable Packaging Material : Recent Innovation and Developments to Remain Environment Friendly and Cost Effective. International Journal of Research in IT, Management and Engineering. 2016; 6, 9-22.
19. Walsh FC, Low CTJ. Surface & Coatings Technology A review of developments in the electrodeposition of tin. Surf. Coat. Technol. 2016; 288, 79-94. https://doi.org/10.1016/j.surfcoat.2015.12.081
20. Gao X, Li W, Ma H. Effect of anti-corrosive performance, roughness and chemical composition of pre-treatment layer on the overall performance of the paint system on cold rolled Steel. Surf. Coat. Technol. 2017; 329, 19-28. https://doi.org/10.1016/j.surfcoat.2017.09.029.
21. Ferrel-Alvarez AC, Lu Y, Ashok A, Subramaniam V, Castaneda H, Electrochemical Characterization of Hot-Dip Galvanized (HDG) Coatings of Zinc-Aluminum and Zinc-Nickel Alloys. J. Mater. Eng. Perform. 2025. https://doi.org/10.1007/s11665-025-11051-6.
22. Walunj MG, Pathak LC, Parida S, Raja VS. Hot dip galvanization of DP 980 steel sheet using iron based sol pre-layer and its corrosion performance. Surf. Coatings Technol. 2025; 504, 132042. https://doi.org/10.1016/j.surfcoat.2025.132042
23. Gupta A, Mishra B. Detinning of Tin-Coated Steel Composite Using Chemical and Electrochemical Techniques. J. Sustain. Metall. 2025; 11, 1237-1249. https://doi.org/10.1007/s40831-025-01047-w
24. Njoku DI, Cui M, Xiao H, Shang B, Li Y. Understanding the anticorrosive protective mechanisms of modified epoxy coatings with improved barrier, active and self-healing functionalities: EIS and spectroscopic Techniques. Sci. Rep. 2017; 7, 1-15. https://doi.org/10.1038/s41598-017-15845-0. PMid:29142312 PMCid:PMC5688088
25. Bo L, Nana C, Jin W, Qianqian L, Junhang C, Jialiang S, Xin Z, Kui X. Corrosion Behavior and Mechanism of Galvalume Steel Sheets in Simulated Acidic Atmosphere Environment. J. Mater. Eng. Perform. 2025; 34, 2775-2787. https://doi.org/10.1007/s11665-024-09300-1
26. Mukherjee R, Badaik S, Pandey AK, Bhagat AN, Rout TK. A hybrid coating of organometallic complex with a silane coupling compound to protect galvannealed (GA) steel from white rust without sacrificing weldability. Mater. Chem. Phys. 2023; 309, 128292. https://doi.org/10.1016/j.matchemphys.2023.128292

27. Kancharla H, Mandal GK, Prasad NK, Vishwanath K, Bhushan B, Godbole K, Singh SS, Mondal K. Effect of inter-critical annealing atmosphere on microstructure and subsequent corrosion behavior of hot-dip galvanized Mn containing high-strength steel. J. Appl. Electrochem. 2024; 54, 1153-1170. https://doi.org/10.1007/s10800-023-02011-w.
28. Kumar P, No-Lee H, Kumar R. Synthesis of phase pure iron oxide polymorphs thin films and their enhanced magnetic properties. J. Mater. Sci. Mater. Electron. 2014; 25, 4553-4561. https://doi.org/10.1007/s10854-014-2203-9
29. Huang BX, Tornatore P, Li YS. IR and Raman spectroelectrochemical studies of corrosion films on tin. Electrochim. Acta. 2001; 46, 671-679. https://doi.org/10.1016/S0013-4686(00)00660-5
30. Song Y, Zhang S, Zhang C, Yang Y, Lv K. Raman spectra and microstructure of zinc oxide irradiated with swift heavy ion. Crystals. 2019; 9, 395. https://doi.org/10.3390/cryst9080395
31. Qiu P, Leygraf C, Odnevall Wallinder I. Evolution of corrosion products and metal release from Galvalume coatings on steel during short and long-term atmospheric exposures. Mater. Chem. Phys. 2012; 133, 419-428. https://doi.org/10.1016/j.matchemphys.2012.01.054
32. Yu K, Xiong Y. Microstructural change of nano grain assemblages with the annealing temperature. Phys. Rev. B - Condens. Matter Mater. Phys. 1997; 55, 2666-2671. https://doi.org/10.1103/PhysRevB.55.2666
33. Raabe D. Texture and microstructure evolution during cold rolling of a strip cast and of a hot rolled austenitic stainless steel. Acta Materialia.1997; 45, 1137-1151. https://doi.org/10.1016/S1359-6454(96)00222-4
34. Ramazani A, Mukherjee K, Schwedt A, Goravanchi P, Prahl U, Bleck W. Quantification of the effect of transformation-induced geometrically necessary dislocations on the flow-curve modelling of dual-phase steels Quantification of the effect of transformation-induced geometrically necessary dislocations on the flow-curve mode. Int. J. Plast. 2013; 43, 128-152. https://doi.org/10.1016/j.ijplas.2012.11.003
35. Yang D, Wang K, Zhou H, Zhang X, Zhang B. Microstructure and properties of galvannealed coatings at different galvannealed time. Mater. Lett. 2023; 345, 134489. https://doi.org/10.1016/j.matlet.2023.134489
36. Shreyas P, Panda B, Kumar R. Materials Today : Proceedings Mechanical properties and microstructure of 316L-galvanized steel weld. Mater. Today Proc. 2020; 23, 600-607. https://doi.org/10.1016/j.matpr.2019.05.418
37. Hu K, Yan X, Qiao D, Du X, Zhang G, Zhao X. Spangle formation on surface of Galvalume steel sheets : Study of microstructure control through cooling dynamics and titanium addition. Vacuum. 2025; 239, 114376. https://doi.org/10.1016/j.vacuum.2025.114376
38. Wint N, Geary S, Mcmurray HN, Williams G, De Vooys ACA. The Kinetics and Mechanism of Atmospheric Corrosion Occurring on Tin and Iron-Tin Intermetallic Coated Steels the Kinetics and Mechanism of Atmospheric Corrosion Occurring on Tin and Iron-Tin Intermetallic Coated Steels. J. Electrochem. Soc. 2015; 162, C775. https://doi.org/10.1149/2.0681514jes
39. Podany P, Gregor T, Studecky T, Donik C. High Manganese TWIP Steel with Increased Corrosion Resistance. Metals (Basel). 2022; 12(10), 1765. https://doi.org/10.3390/met12101765.
40. Gupta AK, Nayak S, Moirangthem RS, Venugopalan T. Bhagat AN, Rout TK. A study on the preparation of passivating surface using bi-layer of nanostructured ZnO and silane functionalized polymer: an alternate option to chromate passivating coating. J. Coatings Technol. Res. 2022; 19, 1101-1115. https://doi.org/10.1007/s11998-021-00588-5
41. Aryanto D, Sudiro T, Wismogroho AS. Correlations between Structural and Hardness of Fe-50%Al Coating Prepared by Mechanical Alloying. Pist. J. Tech. Eng. 2018; 1(2), 1-6. https://doi.org/10.32493/pjte.v1i2.3185.
42. Pandey S, Mishra KK, Ghosh P, Singh AK, Jha SK. Characterization of tin-plated steel. Front. Mater. 2023; 10, 1-10. https://doi.org/10.3389/fmats.2023.1113438
43. Rout TK, Bandyopadhyay N, Venugopalan T. Mechanistic interpretation of electrochemical behaviour of galvannealing coating in saline environment. Corrosion Science. 2005; 47, 2841-2854. https://doi.org/10.1016/j.corsci.2004.11.005
44. Rout TK. Electrochemical impedance spectroscopy study on multi-layered coated steel sheets. Corrosion Science. 2007; 49, 794-817. https://doi.org/10.1016/j.corsci.2006.06.008
45. Ding ZL, Zhang J, Jiang SM, Zhang QF. Effect of magnesium on corrosion resistance of Galvalume coating. J. Phys. Conf. Ser. 2021; 2101, 012078. https://doi.org/10.1088/1742-6596/2101/1/012078
46. Badaik S, Nayak S, Ambade B, Kumar T. Progress in Organic Coatings A novel superior corrosion resistance polyimide - MXene (PI/$Ti_3C_2T_x$) composite coating for low alloy mild steel. Prog. Org. Coatings. 2025; 200, 109046. https://doi.org/10.1016/j.porgcoat.2024.109046
47. Lamiri L, Nessark B. Electrochemical behavior, characterization and corrosion protection properties of poly(bithiophene+2-methylfuran) copolymer coatings on A304 stainless steel. E-Polymers. 2018; 18, 143-151. https://doi.org/10.1515/epoly-2017-0057
48. Sultan BBM, Thierry D, Ogle K. On the dissolution rates and mechanisms of Al-Mg and Al-Cu alloys during acid pickling using element-resolved electrochemistry. Electrochim. Acta. 2023; 444, 141961. https://doi.org/10.1016/j.electacta.2023.141961
49. Yu Y, Guo M, Zhou Y, Jin S, Li B. Performance evaluation of geopolymer anti-corrosion coatings: Synergistic effect of graphene oxide and polydimethylsiloxane. Constr. Build. Mater. 2025; 472, 140871. https://doi.org/10.1016/j.conbuildmat.2025.140871